Potential Role for a Specialized β₃ Integrin-Based Structure On Osteocyte Processes in Bone Mechanosensation

Pamela Cabahug-Zuckerman[1], **Randy F. Stout Jr.**[2,3], **Robert J. Majeska**[1], **Mia M. Thi**[4], **David C. Spray**[3], **Sheldon Weinbaum**[1], and **Mitchell B. Schaffler**[1,*]

[1]Department of Biomedical Engineering, The City College of New York

[2]Department of Biomedical Sciences, New York Institute of Technology College of Osteopathic Medicine

[3]Department of Neuroscience, Albert Einstein College of Medicine

[4]Department of Orthopaedic Surgery, Albert Einstein College of Medicine

Abstract

Osteocyte processes are an order of magnitude more sensitive to mechanical loading than their cell bodies. The mechanisms underlying this remarkable mechanosensitivity are not clear, but may be related to the infrequent $\alpha_V\beta_3$ integrin sites where the osteocyte cell processes attach to canalicular walls. These sites develop dramatically elevated strains during load-induced fluid flow in the lacunar-canalicular system and were recently shown to be primary sites for osteocyte-like MLO-Y4 cell mechanotransduction. These $\alpha_V\beta_3$ integrin sites lack typical integrin transduction mechanisms. Rather, stimulation at these sites alters Ca^{2+} signaling, ATP release and membrane potential. In the current studies, we tested the hypothesis that in authentic osteocytes *in situ*, key membrane proteins implicated in osteocyte mechanotransduction are preferentially localized at or near to β_3 integrin-foci. We analyzed these spatial relationships in mouse bone osteocytes using immunohistochemistry combined with Structured Illumination Super Resolution Microscopy, a method that permits structural resolution at near electron microscopy levels in tissue sections. We discovered that the purinergic channel pannexin1, the ATP-gated purinergic receptor P2X7R and the low voltage transiently opened T-type calcium channel CaV3.2-1 all reside in close proximity to β_3 integrin attachment foci on osteocyte processes, suggesting a specialized mechanotransduction complex at these sites. We further confirmed this observation on isolated osteocytes in culture using STochasitc Optical Resonance Microscopy. These findings identify a possible structural basis for the unique mechanosensation and transduction capabilities of the osteocyte process.

---

*Corresponding Author: Mitchell B. Schaffler, Department of Biomedical Engineering, The City College of New York, 160 Convent Avenue, New York, NY 10031, Telephone: (212) 650-5070, mschaffler@ccny.cuny.edu.

INTRODUCTION

Bone responds to mechanical loading, or its absence, with alterations in architecture and mass [1] [2] [3] [4]. Skeletal responsiveness to physical signals depends on the ability of bone cells to detect those mechanical cues (mechanosensation) and convert them into biochemical events leading to bone formation or resorption (mechanotransduction). There is wide consensus that osteocytes are the primary cells responsible for mechanotransduction in bone [5] [6] [7] [8] [9] [10] [11] [12] [13] [14]. Precisely how osteocytes detect and transduce mechanical signals is not understood, but recent studies point to loading-induced fluid flow in the lacunar-canalicular system (LCS) and resultant forces acting on osteocytes –especially on their dendritic processes - as key elements of the mechanism [8] [9] [15] [16] [17] [18] [19] [20] [21] [22] [23] [24] [25].

That osteocyte cell processes are far more sensitive to mechanical stimuli than their cell bodies has been demonstrated experimentally [22] [26]. Wu *et al.* [22] in our laboratory used a novel fluid loading device to deliver picoNewton level forces to osteocyte processes versus cell bodies and found a sensitivity difference of at least ten-fold. The mechanisms underlying this remarkable mechanosensitivity are not clear, but may be related to sites where the osteocyte cell processes attach to rigid substrata. McNamara *et al.* [27] discovered that osteocyte processes *in situ* attach directly to canalicular walls at apices located 131 ± 40 nm apart, and that these foci were $\alpha_V\beta_3$ integrin attachment sites [27]. These attachment foci – initially identified in rodents but subsequently in human bone [28] – are subject to dramatically elevated strains [20] during load-induced fluid flow in the LCS, leading us to hypothesize that they are primary sites for osteocyte mechanotransduction. Thi *et al.* (2013) [23] confirmed this experimentally; tiny fluid forces applied to attachment foci on osteocyte processes *in vitro* triggered Ca^{2+} signaling that propagated back to cell bodies, while the same stimulus applied away from attachment sites caused no response. Thi *et al.* also found that this Ca^{2+} response was $\alpha_V\beta_3$ integrin-dependent, since it was blocked by disrupting integrin-ligand interactions.

The $\alpha_V\beta_3$ integrin foci along osteocyte process were suggestive of focal adhesion complexes that mediate mechanical responses in numerous cell types. However, these $\alpha_V\beta_3$ integrin sites lack key features of typical integrin transduction mechanisms. Paxillin and vinculin are absent from osteocyte processes [29] (Cabahug *et al.*, unpublished). Furthermore, You *et al.* [30] and Tanaka-Kamioka *et al.* [31] noted that the cytoplasmic space between the osteocyte process membrane and the tightly packed cross-linked actin filament bundles within (<20 nm) is insufficient to accommodate the normal array of adaptor proteins, which typically occupy >40 nm of cytoplasmic depth [28] [30] [32] [33]. Thus, it seems unlikely that typical integrin transduction mechanisms operate in osteocyte processes.

Activation of osteocyte mechanosensors alters several acute membrane-based activities including Ca^{2+} movements, ATP gating and membrane potential [21] [22] [23] [34] [35] [36] [37] [38]. Such responses are mediated by membrane proteins that include the stretch activated purinergic channel pannexin1 (Panx1) [35] [39], the ATP-gated purinergic receptor P2X7R [40] [23], and the low voltage transiently opened T-type calcium channel CaV3.2-1 [21] [36] [37] [41]. The gap junction protein connexin43 (Cx43), has been proposed to

function as an ATP-releasing hemichannel in response to mechanical loading [26] [42], though there is no consensus on this point [43]. Yet regardless of mechanism, osteocyte mechanosensors must necessarily interact with the signal transduction "effector" machinery needed to generate cellular responses. Therefore, we tested the hypothesis that key membrane proteins implicated in osteocyte mechanotransduction are preferentially localized at or near to β_3 integrin-based foci. Our approach was to analyze these spatial relationships, both *in situ* and *in vitro*, with Super Resolution Microscopy methods that permit structural resolution at near electron microscopy levels. We report here that Panx1, P2X7R and CaV3.2-1 all reside in close proximity to β_3 integrin attachment foci, consistent with a specialized mechanotransduction complex. These findings suggest a structural basis for the unique mechanosensation and transduction capabilities of the osteocyte process.

MATERIALS AND METHODS

Candidate molecules

The following proteins were selected for this study: i) Integrin β_3, ii) pannexin1 (Panx1), iii) P2X7R, iv) T-type calcium channel CaV3.2-1 (CaV3), v) connexin43 (Cx43) and vi) vinculin. Each protein was localized by double IHC staining with target ligand vs. combination with β_3 integrin.

Microscopy approaches

Super Resolution Microscopy (SRM) was used to assess the spatial association of candidate proteins with $\alpha_V\beta_3$ integrin attachment foci. Structured Illumination Microscopy or SIM [26] uses conventional fluorophores and can be used on tissue sections. It employs imaging processing approaches to break through the Abbe resolution limit and permits x-y plane resolutions of 85-100 nm [44]. SIM was used for *in situ* co-localization along osteocyte processes in mouse cortical bone tissue sections. TEM [20] [27] showed that the spacing between integrin attachment sites in mouse cortical bone (150±12.4 nm) is sufficient for ligand colocalization by SRM. Direct STochastic Optical Reconstruction Microscopy (dSTORM), which provides better x-y resolution than SIM (20 nm) but cannot penetrate into tissues, was used for studies of isolated osteocytes [44] [45] [46] [47]. Details of SIM and STORM are beyond the scope of this manuscript but are described elsewhere [44] [45] [46] [47] [48].

SIM localization in situ

Under IACUC approval at the City College on New York, 18-week old adult male C57BL/6J mice (JAX, N=6) were euthanized and femurs harvested. Bones were processed and immunohistochemical (IHC) double staining carried out as described by Kennedy [49]. Briefly, bones were fixed in neutral buffered formalin for 48 hours, then decalcified with formic acid, dehydrated in ethylene glycol monoethyl ether (#E180-1, Fisher Scientific), cleared in methyl salicylate (#O3695-500, Fisher Scientific) and then embedded in an ethyl methacrylate (#234893, Sigma Aldrich) resin, which maintains good IHC staining properties and provides excellent retention of microstructure. Diaphyseal 5 μm cross-sections on glass slides were deplasticized, rehydrated and immersed sequentially in 0.3% TritonX100, 10% EDTA and protein blocking reagent (#X0909, Dako Agilent Technologies), 10 min each at

room temperature, then incubated overnight at 4°C with primary antibodies against the two proteins of interest (all antibodies in this study are listed in Table 1). Primary antibody reactivity against Panx1, P2X7R, CaV3, Cx43 was validated in sections of mouse brain; reactivity for antibodies against vinculin and β_3 integrin were established using fibroblasts and osteoclast sealing zones or endothelial cell focal adhesions, respectively. For IHC studies, primary antibodies were diluted with Dako Antibody Diluent (#S3022) at 1:200 and were detected with either Alexafluor488 or Alexafluor568 labeled secondary antibodies (1:700 dilution, room temperature, 30 min). Non-immune, species-appropriate IgGs served as negative controls. After staining, sections were mounted in Eukitt mounting media (EM Sciences) on precision thickness 1.5 glass coverslips (ThermoFisher).

SIM was performed using a Zeiss ELYRA S.1 system equipped with two laser channels; 1-2 μm z-axis image stacks were acquired in 110 nm optical steps (63× oil immersion objective, NA1.4). Both conventional, wide-field fluorescence images and SIM images were simultaneously acquired. The X-Y resolutions in SIM images were 85 nm and 100 nm for AlexaFluor488 (green) and Alexafluor568 (red) dyes, respectively, based on the contrast enhancement grid spacing for each wavelength. Images were acquired (Gain=20, Exposure=100ms) using two tracks to avoid cross-talk between channels, alternating between a red channel (laser excitation 561nm, HR DPSS 561-100 mWatts, 2%; bandpass filter (BP) detection 570-620nm) and a green channel (laser excitation 488 nm, HR Diode 488-100 mWatts, 2%; BP filter detection, 495-550 nm). Images from five rotations and five phase shifts per rotation were processed and de-convolved with Zeiss Zen Black software using raw values of 16-bit image intensities. Channel alignment calibration was performed using multi-excitation nanobeads and image stacks processed with ImageJ (Ver 1.51o,[50]) using unimodal triangulation filtering to remove noise prior to analysis [51]. Analyses were performed on the filtered 16-bit greyscale images.

For initial SIM imaging of osteocytes, mouse femoral diaphyses were stained en bloc in basic fuchsin, which fluoresces at 565 nm excitation. Bones were then embedded in resin and 75 μm thick undecalified cross-sections were cut, polished and cover-slipped for SIM. Using this approach, SIM imaging revealed both osteocytes and their LCS in exquisite detail, both in 3D Z-stack images (Fig 1A) and in single 110 nm thick optical slices like those used for the IHC co-localization studies described below (Fig 1B). A second series of pilot studies validated SIM and IHC imaging and confirmed the canalicular localization of β_3 integrin staining foci [27] using an anti-β_3 antibody (AlexaFluor488 labeled secondary antibody). β_3 integrin foci were observed in canaliculi as well (Fig 1C,D,E). Figure 1F shows a TEM image of the proximal region of a cell process. Even with SIM microscopy, osteocyte cell processes cannot be reliably observed within canaliculi, but we can readily tell where the lacunar edge is located from the unenhanced conventional fluorescence image that the SIM microscope also generates. Thus, we can start our data collection away from that edge in order to sample the osteocyte process.

SIM immunostaining and co-localization studies

Vinculin and β_3 integrin localization *in situ*—Tissue sections were stained simultaneously for β_3 integrin and vinculin, then with secondary antibodies conjugated to

AlexaFluor568 and AlexaFluor488, respectively. Fibroblasts within sections served as positive controls for vinculin staining.

Co-localization of mechanotransduction components with β$_3$ integrin on osteocyte processes *in situ*—IHC double-staining co-localization studies with β$_3$ integrin and specific candidate proteins were performed using antibodies as specified in Table 1.

Image Analysis—SIM images were used for high resolution mapping of β$_3$ integrins and candidate proteins. Analyses were performed using single optical plane images (110nm thick) to avoid distortions that occur in Z-axis reconstructions. [44] [45] [48]. IHC stained foci showed β$_3$ integrins in red (AlexaFluor568), candidate channels in green (AlexaFluor488).

For β$_3$ integrin - vinculin studies, vinculin staining was noted as present or absent, and if present, whether or not it co-localized with β$_3$. For all other β$_3$ integrin-candidate protein pairs, the presence, distribution and degree of co-localization were quantified using ImageJ particle analysis and co-localization indices modules. Fifteen osteocytes per protein pair were chosen from the anterior cortex, >20μm away from periosteal and endosteal surfaces, in 3 non-contiguous sections per animal, a total of 90 osteocytes per animal.

Data collection was performed along all osteocyte processes contained within the section optical plane in concentric elliptical sampling regions of interest spaced 0.5 μm apart and starting 0.5 μm distal to the lacunar margin (Fig 2D). Based on images from previous electron microscopy studies by our laboratory [27] and additional TEM studies (Fig 1F) performed as part of our calibration studies for SIM, the starting point for our data collection (0.5 μm from the lacunar edge) samples the osteocyte process (Fig 1E). Data collection for each process then proceeded outward to 3.5 μm, which was half the mean distance between adjacent lacunae. In each region of interest (ROI), the total area of all stained fluorescing foci was measured for each ligand and divided by the square root of total ROI area.

Protein distribution & co-localization

Manders Coefficients were determined to assess degree of co-localization between fluorescently labeled β$_3$ integrin foci and all candidate proteins using the Coloc2 module in ImageJ with automatic thresholding (Costes methods). The Manders Coefficient M ranges from 0 (no overlap) to 1 (complete overlap). A threshold of M=0.4 or 40% overlap is considered to represent biologically significant co-localization [52] [53] [54] [55]. Manders Coefficients are also directional, such that for two proteins A & B, M_{AB} reflects the fraction of A coinciding with B, while M_{BA}, indicates the fraction of B coinciding with A.

Distances were measured between each of the 6 pairs of membrane proteins with Manders Coefficient >0.4: β$_3$ integrin, CaV3, P2X7R and Panx1. Pairs of red and green foci, were selected, and thirty pairs per osteocyte from an average of 15 cells in each bone section (3 sections per bone) were measured. Each staining locus can be approximated using an Airy function, so an intensity centroid (Fig 2E) can be determined and the distance measured from centroid to centroid using this approach. Distances were determined using ImageJ.

Localization of osteocyte process mechanotranduction apparatus in isolated osteocytes using STORM

Direct STochastic Optical Reconstruction Microscopy (dSTORM) was used to examine co-localization of the candidate proteins on cell processes of isolated osteocytes. dSTORM provides resolution of 20 nm for cells on cover slips. In addition, dSTORM can image multiple wavelengths, allowing us to test for extremely precise co-localization among our candidate proteins. MLO-Y4 osteocytes were grown for 7 days on collagen-coated #1.5 glass coverslips (MatTek Corporation); cells were cultured in α-MEM supplemented with 5% FBS, 2.5% bovine serum and 1% Penicillin-Streptomycin. Cells were co-transfected with two plasmids: one plasmid contained the gene for mouse Panx1 with an mCherry tag (pLenti6V5-EF1a-mPanx1-mCherry) and the other contained mouse β_3-integrin with a 3X-flag epitope tag on the integrin, using Optifect as per manufacturer protocol. A transfection approach to create fluorescent proteins provides higher spatial precision than antibody approaches – the constructs are much smaller which allows improved resolution in the resulting reconstructed images. Cells were washed with PBS and fixed for 20 min in 4% paraformaldehyde in PBS. Cells were then washed and blocked in 2% donkey serum and 0.4% Triton-X 100 in PBS for 30 min at room temperature. Cells were incubated with primary antibodies overnight at 4°C, then washed and incubated with secondary antibodies for 1 hour. STORM image acquisition and processing were performed as follows: Freshly prepared buffer 50mM Tris, 10% w/v Glucose, Glucose Oxidase mix (0.5mg/ml glucose oxidase, 40μg/ml Catalase) and 100mM β-Mercaptoethylamine was placed on cells to induce mCherry blinking [56]. Images were acquired using a Nikon N-STORM microscope (Nikon Instruments, Melville NY) with a 100× magnification oil objective. 2-dimensional images were acquired (100% laser power for all three excitation wavelengths- 488nm, 560nm, and 647nm) and exposure time set to 30ms. dSTORM images were processed using Nikon Elements N-STORM software with the overlapping peak recognition algorithm. Localized molecules were displayed as Gaussian spots and spot brightness and diameter determined by localization precision. In-software drift correction and correction for chromatic aberration (based on prior calibration using a fluorescent bead standard) was applied to reconstructions. We employed a density filter in order to eliminate background secondary fluorescence: only molecules localized in clusters with a molecule count of 15 within an 80 nm distance were displayed in the image shown in Figure 7. For cluster analysis, a density filter of 5 localizations within 80 nm was used. β_3 integrin clusters were defined by inclusion of only the localizations that had 5 or more other localizations within 80 nm of the centroid for each localization being tested for inclusion in a cluster. After all localizations were tested for inclusion within a cluster, those that did not meet cluster criteria were removed from the list of localizations and the reconstructed dSTORM image used for further analysis.

Statistical analyses

Data for protein distribution and pair co-localization from SIM studies are reported as means ± standard deviation. SPSS (IBM, Ver 20) was used for analysis. Two-way ANOVA tested for differences among the membrane proteins examined along each region of the osteocyte processes and between regions for each protein. Post hoc Fisher's least significant difference test was used to perform pairwise comparisons for each of the three candidate channels with

β$_3$ and each other, at each region along the osteocyte processes. Tukey's test was used to determine differences between all groups. Significance is reported at p<0.05.

RESULTS

Analysis of osteocyte mechanotranduction proteins on osteocyte processes in situ by SIM

Double IHC staining for β$_3$ integrin and vinculin (Fig 3) showed that vinculin was present in osteocyte cell bodies but absent from osteocyte processes. In contrast, β$_3$ integrin was also present beyond the lacuna margin. There was no overlap between vinculin and β$_3$ integrins.

Double IHC staining for β$_3$ integrin in combination with Panx1, P2X7R and CaV3 and Cx43 revealed that all of these proteins were located along osteocyte processes (Fig 2). Distributions of β$_3$ integrin, P2X7R, Panx1 and CaV3 along the processes were similar; highest concentrations of these ligands were near the origin of the osteocyte process, declining over the first 1.5 μm from the lacunar margin. After that point, levels for all of these proteins remained low and relatively constant along the length of the process (Fig 4). In contrast, Cx43 staining was present only at extremely low levels and was uniformly distributed along the length of osteocyte (Fig 2H).

Co-localization of candidate proteins

In the proximal regions of osteocyte process, within 1 μm from the lacunar margin, Manders Coefficients for the association of Panx1, P2X7R and CaV3 with β$_3$ foci ranged from 0.6-0.9 (Fig 5A) showing that the majority of these molecules strongly co-localize with β$_3$ integrin foci in this region. At greater distances from the lacunar margin, Manders coefficients declined continuously so that at distances above 2 μm from the lacunae, all M values were below the threshold level (0.4) for positive association. However, all of these proteins exhibited M values for association with β$_3$ integrin that were greater than seen for Cx43, which invariably averaged less than 0.1, indicating that it is not part of the Panx1, P2X7R, CaV3, β$_3$ complex.

Reverse Manders coefficients, indicating the association of β$_3$ integrin with other proteins, showed qualitatively similar patterns, declining with distance from the lacunar margin (Fig 5B). However, the reverse coefficients in proximal regions of the processes near the cell body were lower than the forward coefficients. This finding indicates that not all β$_3$ sites are associated with the candidate proteins. Cx43 was not spatially associated with β$_3$ integrin sites at any location along osteocyte processes. Finally, at all regions examined, the M values between β$_3$ integrin and Panx1, P2X7R and CaV3 were similar to each other (p>0.20), in contrast to the lack of association with Cx43 (p<0.05).

Distances between all pairwise combinations of membrane proteins examined in regions where Manders coefficients were greater than 0.4 ranged from 40-87 nm, with P2X7R and Panx1 being in closest proximity to each other (Fig 6).

Analysis of the osteocyte mechanotransduction proteins in MLO-Y4 cells by STORM

Spatial relationships among β$_3$ integrin, P2X7R and Panx1 were assessed in isolated osteocytes. β$_3$ integrin foci were readily visualized along the processes of MLO-Y4

osteocytes (Fig 7), and were punctate in distribution along the cell processes, similar to our *in situ* SIM findings. These larger foci were comprised of smaller staining units, consistent with the well-known clustering of β_3 integrins at adhesion sites. β_3 integrin foci was found to colocalize with Panx1-mCherry and endogenous P2X7Rs in multiple cell processes extending from the cells.. We characterized spacing and co-clustering of the molecules instead of Mander's coefficient analysis because colocalization of signal in reconstructed dSTORM images is not a useful statistic due to the point-based nature of this localization microscopy. For co-cluster estimation with β_3 integrin clusters, we examined 11 processes on each of seven different cells. Co-clustering was categorized as those β_3 integrin clusters having one or more localization of a β_3 integrin or another mechanosensor protein localization within 80 nm. The majority of β_3 integrin clusters (~60%) were found within 80 nm of P2X7R and/or Panx1, and some 23% of integrin clusters had these proteins within the cluster. Some of the β_3 foci were not associated with channel proteins (not shown), consistent with findings in the SIM-based Manders co-localization studies described.

DISCUSSION

In this study, SIM-based super-resolution microscopy was used to determine with high resolution, the spatial relationships between β_3 integrin, a likely mechanosensory molecule, and a set of membrane channel proteins and receptors implicated in osteocyte mechanotransduction. The results revealed that the β_3 integrin foci on osteocyte processes are co-localized (at distances <90 nm) with the ATP-releasing Pannexin 1 (Panx1) channel, the P2X7R purinergic receptor and ligand gated CaV3 calcium channels. However, we found no *in situ* association between $\alpha_V\beta_3$ integrins and the gap junction protein Cx43, whose hemichannels were shown to mediate mechanosensitive ATP release in osteocyte-like cells *in vitro* [26] [42].

Recent discoveries strongly support the concept that the remarkable mechanosensitivity of osteocytes is based in their cell processes, i.e., their "fingers". The experimental demonstration by Wu *et al.* [22] in our laboratory that fluid forces of about 10 picoNewton on osteocyte processes triggered voltage changes in osteocytes, while forces 10-20 times higher were needed to directly stimulate osteocyte cell bodies, suggested that the processes possess specialized mechanosensitive structures not present in their bodies. McNamara *et al.* [27] in our laboratory discovered that osteocyte processes *in situ* attach directly to projections from canalicular walls at foci located approximately ~150 nm apart, a finding subsequently confirmed in human bone as well [28]. Furthermore, we found these sites on the processes were $\alpha_V\beta_3$ integrin attachment foci, while β_1 based integrins dominated on osteocyte cell bodies. Wang *et al.* [20] developed a mathematical model showing that membrane strains at these integrin attachment foci along osteocyte processes are at least an order of magnitude greater than whole-tissue strains in loaded bone. In other words, the focal attachments of osteocyte processes to canalicular walls act like stress concentrations to amplify membrane strains, so that tiny forces on the process produce local membrane strains at those sites large enough to trigger a range of first order signaling processes (e.g., ATP, Ca^{2+} and PGE_2). Thi *et al.* in our group [23] confirmed this hypothesis, finding that tiny fluid forces applied to attachment foci on osteocyte processes *in vitro* triggered Ca^{2+} signaling that propagated back to the cells bodies, while the same stimulus applied away from

attachment sites caused no response. Furthermore, Ca^{2+} signaling response evoked by fluid loading at the osteocyte process attachment foci depends on β_3 integrins and ATP release.

Both β_1 and β_3 integrins have been implicated in osteocyte mechanotransduction *in vitro* and *in vivo* [23] [24] [25] [41] [57] [58] [59]. β_1 integrins on osteocyte cell bodies may be involved in responses to large deformations [26] [59] [60]. Indeed, Jiang and co-workers showed *in vitro* that stretch on β_1 integrins of MLO-Y4 cells opens hemichannels and releases ATP [26]. However, the mechanical stimulus used in these studies was far larger than osteocyte cell bodies can experience *in vivo*, so it is difficult to extrapolate from these findings. Moreover, recent *in vivo* studies on cell-specific deletion of β_1 integrin in mice bone showed that β_1 integrins play a central role in osteoblastogenesis and bone development, but do not appear to contribute substantially to adult bone mechanotransduction [61]. In contrast, several studies show that mechanotransduction in osteocytes depends substantially upon β_3 integrins *in vitro* [23] [25] [41].

Mechanotransduction mechanisms at typical $\alpha_V\beta_3$ integrin–based focal adhesion sites are well understood. However, the $\alpha_V\beta_3$ integrin foci on osteocyte processes have unusual features which suggest that typical integrin mechanotransduction mechanisms are likely not in play here. In typical mechanically active focal adhesion complexes, the cytoplasmic domains of the α and β integrins subunits attach to a large complex of cytoplasmic adaptor and signaling proteins (e.g., talin, vinculin, paxillin, focal adhesion kinase and many more) which in turn attach to the loose, subcortical actin web in order to transduce the mechanical signals into biomechanical signals [62] [63]. Osteocyte processes are filled with a dense, tightly packed bundle of highly cross-linked parallel actin fibers [28] [30] that leaves little if any cytoplasmic space to accommodate the large array of cytoplasmic adaptor proteins at typical focal adhesion sites. Vatsa *et al.* [29] found no paxillin in osteocyte processes, but it was present in cell bodies where a looser actin web and sufficient space exist [16] [20] [64] [65]. Similarly, we found that vinculin was absent from osteocyte processes but was readily demonstrable in their cell bodies. Thus, the $\alpha_V\beta_3$ integrin foci along osteocyte processes do not appear to be part of typical integrin-based mechanotransductive focal adhesions.

These studies reveal that the Panx1 channel is co-localized with the integrin foci on osteocyte processes, both *in situ* and *in vitro*. Panx1 is known to provide a conduit for controlled cellular ATP release in numerous cell types including bone cells. Panx1 is a member of the pannexin family of transmembrane channel-forming proteins and is widely expressed in all tissues [66]. Pannexins are the mammalian homologues to the invertebrate gap junction proteins, the innexins. However, pannexins, including Panx1, form only non-junctional channels, i.e., "hemichannels", that allow exchange of small molecules between the cytoplasm and the extracellular space [43] [67] [68]. Panx1 channels are voltage sensitive [69] [70]. Critically for osteocyte mechanotransduction, they also open in response to mechanical stretch [35], elevation in extracellular K^+ and activation of cell surface receptors, in particular the ionotropic P2X7R [71] [72]. We also found that the P2X7R purinergic receptor colocalized with β_3 integrin attachment sites on osteocyte processes, which points to a spatial as well as functional coupling for the purinergic signals released from Panx1 channels and their binding to nearby P2X7R in the progression of mechanotransduction. These findings were evident in both *in vitro* and in authentic

osteocytes *in situ*. It is well established that purinergic signaling is required for normal bone growth and adaptation [40]. The T-type calcium channel CaV3 was also found to be associated with the β_3 integrin-Panx1-P2X7R complex *in situ*. This channel has been shown to be affected by stretch activated ATP release [21], and also by membrane depolarization by the stretch activated Panx1 channel [35] [38].

The principal focus of the current study was to test for the presence and colocalization of β_3 integrin and channel proteins on osteocyte cell processes. Some cell body staining for β_3 integrin, Panx1, P2X7R and CaV3 was also observed, which would be expected for the obligate site of synthesis for these proteins. Indeed, it would have been surprising to have not found these proteins in osteocyte cell bodies. The current high-resolution imaging studies could not directly address function of these proteins at the cell body. However, we can make strong inferences. Principally, the β_3 integrins on osteocyte cell bodies *in situ* cannot function as fixed mechanical anchor points that would generate elevated membrane strains as they do on osteocyte processes. β_3 integrins on osteocyte process membranes attach directly to the canalicular wall, with effectively no space between them [27] [28]. In contrast, β_3 integrins on osteocyte cell bodies cannot bridge the wide extracellular space (0.5-1 μm) that surrounds osteocyte bodies. Without anchoring to the bone, the β_3 integrins on cell bodies would be unable to generate sufficiently high membrane strains to open stretch activated channels such as Panx1 [20]. Thus, it seems reasonable to posit that when present on osteocyte cell bodies, β_3 and the candidate channel proteins either function in other capacities or are in transit to other locations, e.g. cell processes.

The current studies are the first to our knowledge, to employ SIM super-resolution microscopy approaches to interrogate the structure of bone tissue osteocytes in their native environment. This allowed us to distinguish between protein foci in close proximity to the β_3 integrin foci on osteocyte processes of authentic osteocytes *in situ*. The SIM system used however, only has two lasers and so our studies were limited to double staining assays. STORM based assessments on isolated osteocytes allowed us to interrogate more than two proteins, and at resolutions typically associated with electron microscopy approaches. With both approaches, we found that Panx1 channel, P2X7R purinergic ligand gated and CaV3 calcium channels are clustered within ~60 nm of each other and within less than 90 nm of the β_3 integrin attachment sites. Based on the Wang *et al.* [20] mathematical model for strain amplification, loading in the range of 20 MPa, as occurs with light jogging or fast walking, will cause membrane areal displacements of approximately $2nm^2$ at a distance of 100 nm from an osteocyte process $\alpha_V\beta_3$ integrin attachment site. This membrane strain level has been shown to be sufficient to open stretch activated potassium channels in neuronal cells [73]. Panx1 mechanosensitivity sits well within the elevated strain region of the osteocyte process membrane.

Among the most surprising findings of these studies was the high concentration of the osteocyte mechanotransduction complexes within the first 1.5-2 μm of osteocyte process. It should be noted, however, that these osteocyte mechanotransduction complexes were also found more distally along the process. Why these mechanotransduction complexes are concentrated in the proximal ~ 15% of the osteocyte process is unclear at this time. However, the proximal region of the process is nearest to the site of protein production.

Since osteocyte processes contain a highly cross-linked (i.e., low turnover) actin bundle and lack a microtubule transport system, effective transport of channel protein clusters to more distal regions of cell processes is likely to be slow, possibly resulting in buildups in the more proximal regions. Further engineering modeling studies are needed to understand whether the local mechanical forces to which this region is subjected differ from those further distally along the process. Irrespective of how and why this arrangement arises, these data reveal a hitherto unrecognized functional polarization in osteocyte processes *in situ* and suggest that osteocyte processes may have a major "business end" for mechanosensing.

In summary, the current studies reveal that β_3 integrin foci on the osteocyte process anchor a novel transduction complex, or "osteocyte mechanosome" which may explain the remarkable mechanosensitivity of osteocytes cell processes and the dependency of this sensitivity on ATP-based signaling. We propose the following model: During loading-induced fluid flow in the LCS, $\alpha_V\beta_3$ integrins attaching to process membrane to the canalicular wall become sites of membrane stress (strain) concentrations. The current studies showed that these β_3 integrin foci co-localize with the ATP-releasing Panx1 channel, the P2X7R channel complex and the T-type CaV3 calcium channel. Mechanistically, we speculate that ATP release occurs through the localized stretch activation of Panx1 channels. This ATP binds to the P2X7R complex, which undergoes a conformational change to allow Ca^{2+} influx. The consequent depolarization of the cell process membrane triggers the activation of T-type channel CaV3 causing more calcium ions to enter the cell, thereby sending waves of calcium signaling that summate in the direction towards the osteocyte cell body. While functional and molecular details need to be further elucidated, our data and model are consistent with the experimental loading studies of osteocyte processes *in vitro* reported by us in Thi *et al* [23], who found that the unique and exquisite sensitivity of osteocyte processes depends on a β_3 integrin complex and works through an ATP release that triggers calcium signaling. We further posit that this unique mechanotransduction complex might be targeted pharmacologically to alter mechanosensitivity of bone, and thereby improve or maintain structural integrity of bone.

Acknowledgments

References

1. Globus RK, Bikle DD, Morey-Holton E. The temporal response of bone to unloading. Endocrinology. 1986; 118(2):733–42. [PubMed: 3943489]

2. Krahl H, et al. Stimulation of bone growth through sports. A radiologic investigation of the upper extremities in professional tennis players. Am J Sports Med. 1994; 22(6):751–7. [PubMed: 7856798]

3. Turner CH, Pavalko FM. Mechanotransduction and functional response of the skeleton to physical stress: the mechanisms and mechanics of bone adaptation. J Orthop Sci. 1998; 3(6):346–55. [PubMed: 9811988]

4. Burr DB, Robling AG, Turner CH. Effects of biomechanical stress on bones in animals. Bone. 2002; 30(5):781–6. [PubMed: 11996920]

5. Doty SB. Morphological evidence of gap junctions between bone cells. Calcif Tissue Int. 1981; 33(5):509–12. [PubMed: 6797704]

6. Pead MJ, et al. Increased 3H-uridine levels in osteocytes following a single short period of dynamic bone loading in vivo. Calcif Tissue Int. 1988; 43(2):92–6. [PubMed: 3142673]

7. Palumbo C, Palazzini S, Marotti G. Morphological study of intercellular junctions during osteocyte differentiation. Bone. 1990; 11(6):401–6. [PubMed: 2078434]

8. Weinbaum S, Cowin SC, Zeng Y. A model for the excitation of osteocytes by mechanical loading-induced bone fluid shear stresses. J Biomech. 1994; 27(3):339–60. [PubMed: 8051194]

9. Klein-Nulend J, et al. Sensitivity of osteocytes to biomechanical stress in vitro. FASEB J. 1995; 9(5):441–5. [PubMed: 7896017]

10. Burger EH, et al. Function of osteocytes in bone–their role in mechanotransduction. J Nutr. 1995; 125(7 Suppl):2020S–2023S. [PubMed: 7602386]

11. Mullender MG, Huiskes R. Osteocytes and bone lining cells: which are the best candidates for mechano-sensors in cancellous bone? Bone. 1997; 20(6):527–32. [PubMed: 9177866]

12. Tatsumi S, et al. Targeted ablation of osteocytes induces osteoporosis with defective mechanotransduction. Cell Metab. 2007; 5(6):464–75. [PubMed: 17550781]

13. Bonewald LF. The amazing osteocyte. J Bone Miner Res. 2011; 26(2):229–38. [PubMed: 21254230]

14. Schaffler MB, et al. Osteocytes: master orchestrators of bone. Calcif Tissue Int. 2014; 94(1):5–24. [PubMed: 24042263]

15. Weinbaum S, Guo P, You L. A new view of mechanotransduction and strain amplification in cells with microvilli and cell processes. Biorheology. 2001; 38(2-3):119–42. [PubMed: 11381170]

16. You LD, et al. A model for strain amplification in the actin cytoskeleton of osteocytes due to fluid drag on pericellular matrix. Journal of Biomechanics. 2001; 34(11):1375–1386. [PubMed: 11672712]

17. Cowin SC. Mechanosensation and fluid transport in living bone. J Musculoskelet Neuronal Interact. 2002; 2(3):256–60. [PubMed: 15758447]

18. Reilly GC, et al. Fluid flow induced PGE(2) release by bone cells is reduced by glycocalyx degradation whereas calcium signals are not. Biorheology. 2003; 40(6):591–603. [PubMed: 14610310]

19. Han YF, et al. Mechanotransduction and strain amplification in osteocyte cell processes. Proceedings of the National Academy of Sciences of the United States of America. 2004; 101(47): 16689–16694. [PubMed: 15539460]

20. Wang YL, et al. A model for the role of integrins in flow induced mechanotransduction in osteocytes. Proceedings of the National Academy of Sciences of the United States of America. 2007; 104(40):15941–15946. [PubMed: 17895377]

21. Thompson WR, et al. Association of the alpha(2)delta(1) subunit with Ca(v)3.2 enhances membrane expression and regulates mechanically induced ATP release in MLO-Y4 osteocytes. J Bone Miner Res. 2011; 26(9):2125–39. [PubMed: 21638318]

22. Wu D, et al. On the electrophysiological response of bone cells using a Stokesian fluid stimulus probe for delivery of quantifiable localized picoNewton level forces. Journal of Biomechanics. 2011; 44(9):1702–1708. [PubMed: 21511259]

23. Thi MM, et al. Mechanosensory responses of osteocytes to physiological forces occur along processes and not cell body and require alphaVbeta3 integrin. Proc Natl Acad Sci U S A. 2013; 110(52):21012–7. [PubMed: 24324138]

24. Kaneko K, et al. Integrin alphav in the mechanical response of osteoblast lineage cells. Biochem Biophys Res Commun. 2014; 447(2):352–7. [PubMed: 24726648]

25. Haugh MG, Vaughan TJ, McNamara LM. The role of integrin alpha(V)beta(3) in osteocyte mechanotransduction. J Mech Behav Biomed Mater. 2015; 42:67–75. [PubMed: 25460927]

26. Batra N, et al. Mechanical stress-activated integrin alpha5beta1 induces opening of connexin 43 hemichannels. Proc Natl Acad Sci U S A. 2012; 109(9):3359–64. [PubMed: 22331870]

27. McNamara LM, et al. Attachment of osteocyte cell processes to the bone matrix. Anat Rec (Hoboken). 2009; 292(3):355–63. [PubMed: 19248169]

28. Kamioka H, et al. Microscale fluid flow analysis in a human osteocyte canaliculus using a realistic high-resolution image-based three-dimensional model. Integrative Biology. 2012; 4(10):1198–1206. [PubMed: 22858651]

29. Vatsa A, et al. Paxillin localisation in osteocytes-Is it determined by the direction of loading? Biochemical and Biophysical Research Communications. 2008; 377(4):1019–1024. [PubMed: 18187040]

30. You LD, et al. Ultrastructure of the osteocyte process and its pericellular matrix. Anatomical Record Part a-Discoveries in Molecular Cellular and Evolutionary Biology. 2004; 278a(2):505–513.

31. Tanaka-Kamioka K, et al. Osteocyte shape is dependent on actin filaments and osteocyte processes are unique actin-rich projections. J Bone Miner Res. 1998; 13(10):1555–68. [PubMed: 9783544]

32. Kanchanawong P, et al. Nanoscale architecture of integrin-based cell adhesions. Nature. 2010; 468(7323):580–U262. [PubMed: 21107430]

33. Kuo JC, et al. Isolation of Focal Adhesion Proteins for Biochemical and Proteomic Analysis. Integrin and Cell Adhesion Molecules: Methods and Protocols. 2011; 757:297–323.

34. Mobasheri A, et al. Integrins and stretch activated ion channels; putative components of functional cell surface mechanoreceptors in articular chondrocytes. Cell Biology International. 2002; 26(1):1–18. [PubMed: 11779216]

35. Bao L, Locovei S, Dahl G. Pannexin membrane channels are mechanosensitive conduits for ATP. Febs Letters. 2004; 572(1-3):65–68. [PubMed: 15304325]

36. Shao Y, Alicknavitch M, Farach-Carson MC. Expression of voltage sensitive calcium channel (VSCC) L-type Cav1.2 (alpha1C) and T-type Cav3.2 (alpha1H) subunits during mouse bone development. Dev Dyn. 2005; 234(1):54–62. [PubMed: 16059921]

37. Kudirka JC, et al. P2Y nucleotide receptor signaling through MAPK/ERK is regulated by extracellular matrix: Involvement of beta 3 integrins. Journal of Cellular Physiology. 2007; 213(1):54–64. [PubMed: 17620283]

38. Beckel JM, et al. Mechanosensitive Release of Adenosine 5′-triphosphate Through Pannexin Channels and Mechanosensitive Upregulation of Pannexin Channels in Optic Nerve Head Astrocytes: A Mechanism for Purinergic Involvement in Chronic Strain. Glia. 2014; 62(9):1486–1501. [PubMed: 24839011]

39. Locovei S, Bao L, Dahl G. Pannexin 1 in erythrocytes: Function without a gap. Proceedings of the National Academy of Sciences of the United States of America. 2006; 103(20):7655–7659. [PubMed: 16682648]

40. Li J, et al. The P2X7 nucleotide receptor mediates skeletal mechanotransduction. J Biol Chem. 2005; 280(52):42952–9. [PubMed: 16269410]

41. Miyauchi A, et al. AlphaVbeta3 integrin ligands enhance volume-sensitive calcium influx in mechanically stretched osteocytes. J Bone Miner Metab. 2006; 24(6):498–504. [PubMed: 17072743]

42. Genetos DC, et al. Oscillating fluid flow activation of gap junction hemichannels induces ATP release from MLO-Y4 osteocytes. Journal of Cellular Physiology. 2007; 212(1):207–214. [PubMed: 17301958]

43. Thi MM, et al. Connexin43 and Pannexin1 Channels in Osteoblasts: Who Is the "Hemichannel"? Journal of Membrane Biology. 2012; 245(7):401–409. [PubMed: 22797941]

44. Gustafsson MGL. Surpassing the lateral resolution limit by a factor of two using structured illumination microscopy. Journal of Microscopy-Oxford. 2000; 198:82–87.

45. Heintzmann R, Ficz G. Breaking the resolution limit in light microscopy. Digital Microscopy, 3rd Edition. 2007; 81:561–+.

46. Gustafsson MGL, et al. Three-dimensional resolution doubling in wide-field fluorescence microscopy by structured illumination. Biophysical Journal. 2008; 94(12):4957–4970. [PubMed: 18326650]

47. Huang B, Babcock H, Zhuang XW. Breaking the Diffraction Barrier: Super-Resolution Imaging of Cells. Cell. 2010; 143(7):1047–1058. [PubMed: 21168201]

48. Schermelleh L, Heintzmann R, Leonhardt H. A guide to super-resolution fluorescence microscopy. Journal of Cell Biology. 2010; 190(2):165–175. [PubMed: 20643879]

49. Kennedy OD, et al. Osteocyte apoptosis is required for production of osteoclastogenic signals following bone fatigue in vivo. Bone. 2014; 64:132–137. [PubMed: 24709687]

50. Schneider CA, R WS, Elicieri KW. NIH Image to ImageJ: 25 years of image analysis. Nature Methods. 2012; 9(7):671–675. [PubMed: 22930834]

51. Rosin PL. Unimodal thresholding. Pattern Recognition. 2001; 34(11):2083–2096.

52. Manders EMM, Verbeek FJ, Aten JA. Measurement of Colocalization of Objects in Dual-Color Confocal Images. Journal of Microscopy-Oxford. 1993; 169:375–382.

53. Zinchuk V, Zinchuk O, Okada T. Quantitative colocalization analysis of multicolor confocal immunofluorescence microscopy images: Pushing pixels to explore biological phenomena. Acta Histochemica Et Cytochemica. 2007; 40(4):101–111. [PubMed: 17898874]

54. Dunn KW, Kamocka MM, McDonald JH. A practical guide to evaluating colocalization in biological microscopy. Am J Physiol Cell Physiol. 2011; 300(4):C723–42. [PubMed: 21209361]

55. Zinchuk V, Wu Y, Grossenbacher-Zinchuk O. Bridging the gap between qualitative and quantitative colocalization results in fluorescence microscopy studies. Scientific Reports. 2013; 3

56. Winterflood CM, Ewers H. Single-Molecule Localization Microscopy using mCherry. Chemphyschem. 2014; 15(16):3447–3451. [PubMed: 25111075]

57. Weyts FAA, et al. ERK activation and alpha v beta 3 integrin signaling through Shc recruitment in response to mechanical stimulation in human osteoblasts. Journal of Cellular Biochemistry. 2002; 87(1):85–92. [PubMed: 12210725]

58. Plotkin LI, et al. Mechanical stimulation prevents osteocyte apoptosis: requirement of integrins, Src kinases, and ERKs. American Journal of Physiology-Cell Physiology. 2005; 289(3):C633–C643. [PubMed: 15872009]

59. Litzenberger JB, et al. Beta1 integrins mediate mechanosensitive signaling pathways in osteocytes. Calcif Tissue Int. 2010; 86(4):325–32. [PubMed: 20213106]

60. Pommerenke H, et al. The mode of mechanical integrin stressing controls intracellular signaling in osteoblasts. J Bone Miner Res. 2002; 17(4):603–11. [PubMed: 11918217]

61. Shekaran A, et al. The effect of conditional inactivation of beta 1 integrins using twist 2 Cre, Osterix Cre and osteocalcin Cre lines on skeletal phenotype. Bone. 2014; 68:131–141. [PubMed: 25183373]

62. Banes AJ, et al. Mechanoreception at the cellular level: The detection, interpretation, and diversity of responses to mechanical signals. Biochemistry and Cell Biology-Biochimie Et Biologie Cellulaire. 1995; 73(7-8):349–365. [PubMed: 8703408]

63. Geiger B, Yamada KM. Molecular architecture and function of matrix adhesions. Cold Spring Harb Perspect Biol. 2011; 3(5)

64. Thi MM, et al. The role of the glycocalyx in reorganization of the actin cytoskeleton under fluid shear stress: a "bumper-car" model. Proc Natl Acad Sci U S A. 2004; 101(47):16483–8. [PubMed: 15545600]

65. Galbraith CG, Yamada KM, Galbraith JA. Polymerizing actin fibers position integrins primed to probe for adhesion sites. Science. 2007; 315(5814):992–5. [PubMed: 17303755]

66. Penuela S, Gehi R, Laird DW. The biochemistry and function of pannexin channels. Biochim Biophys Acta. 2013; 1828(1):15–22. [PubMed: 22305965]

67. Bruzzone R, et al. Pannexins, a family of gap junction proteins expressed in brain. Proc Natl Acad Sci U S A. 2003; 100(23):13644–9. [PubMed: 14597722]

68. Wang J, Dahl G. SCAM analysis of Panx1 suggests a peculiar pore structure. J Gen Physiol. 2010; 136(5):515–27. [PubMed: 20937692]

69. Bunse S, et al. The potassium channel subunit Kvbeta3 interacts with pannexin 1 and attenuates its sensitivity to changes in redox potentials. FEBS J. 2009; 276(21):6258–70. [PubMed: 19780818]

70. Iglesias RM, Spray DC. Pannexin1-Mediated ATP Release Provides Signal Transmission Between Neuro2A Cells. Neurochemical Research. 2012; 37(6):1355–1363. [PubMed: 22359052]

71. Iglesias R, et al. P2X7 receptor-Pannexin1 complex: pharmacology and signaling. Am J Physiol Cell Physiol. 2008; 295(3):C752–60. [PubMed: 18596211]

72. Isakson BE, Thompson RJ. Pannexin-1 as a potentiator of ligand-gated receptor signaling. Channels. 2014; 8(2):118–123. [PubMed: 24576994]

73. Honore E, et al. Desensitization of mechano-gated K2P channels. Proc Natl Acad Sci U S A. 2006; 103(18):6859–64. [PubMed: 16636285]
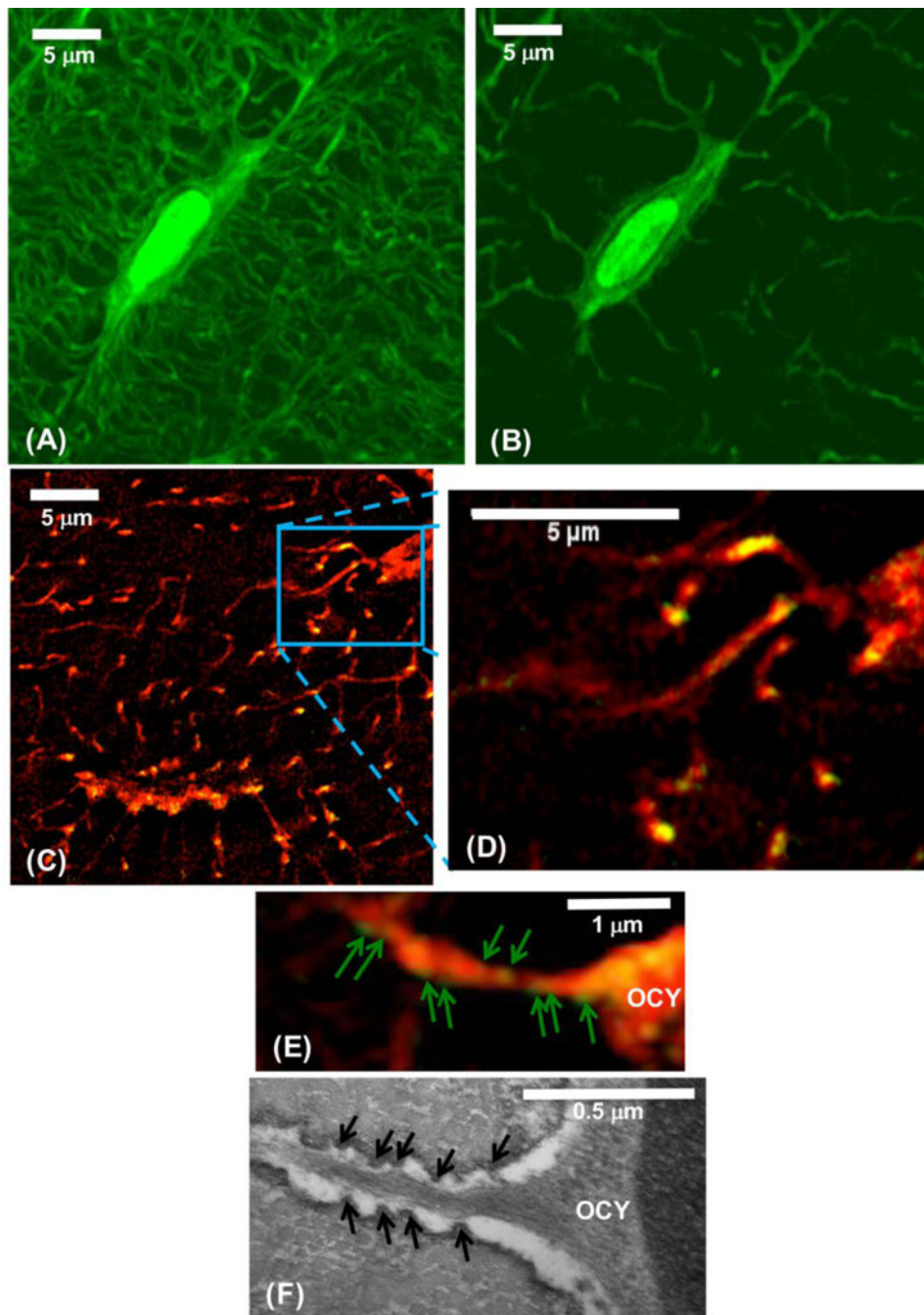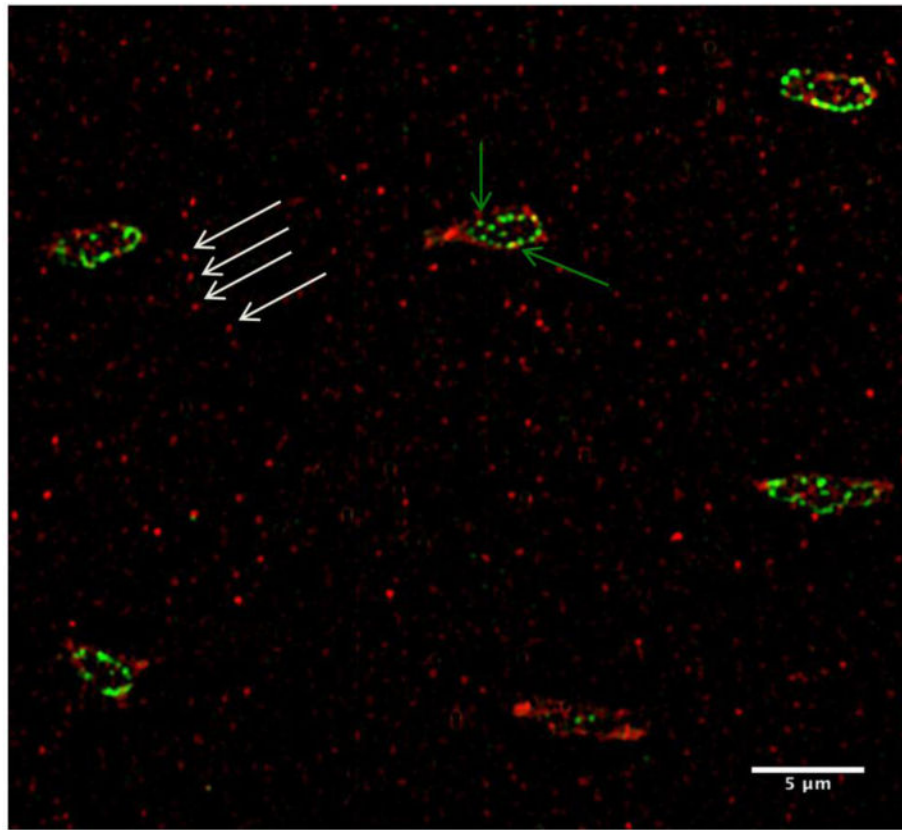
Figure 1.
(A) SIM image showing a 3 μm thick z-stack projection of an osteocyte, its lacuna and canaliculi in mouse cortical bone (basic fuchsin fluorescence, 565 nm excitation, pseudocolored green for visualization, x-y resolution ~100 nm). **(B)** shows a single 110 nm thick SIM optical section from the osteocyte shown in **A**. This image reveals that the osteocyte is separated from the lacunar wall by an ~ 0.5 μm wide pericellular space, consistent with findings from electron microscopy studies [27] [28] [30]. Note that most of the canaliculi appear discontinuous in these very thin optical sections, as they go in and out

of the plane of the section due to their tortuous course through bone. **(C, D)** Projection (1 μm z-stack) SIM image of bone stained for β_3 integrin (Green, Alexa488) and counter-stained with basic fuchsin (Red). **(E)** Enlarged SIM image of single canaliculus (1 μm z-stack image) showing IHC staining of β_3 integrin foci (green arrows) within; yellow/orange foci indicate where the green stained β_3 integrin co-localizes with the red-fluorescing fuchsin dye. **(F)** TEM photomicrograph of an osteocyte showing the cell body (OCY) and the proximal region of the cell process, similar to the SIM image in **E**. Projections from the canalicular wall (black arrows) to the cell process are the attachment foci for the β_3 integrins; these projections are not present on lacunar walls [27] [28].
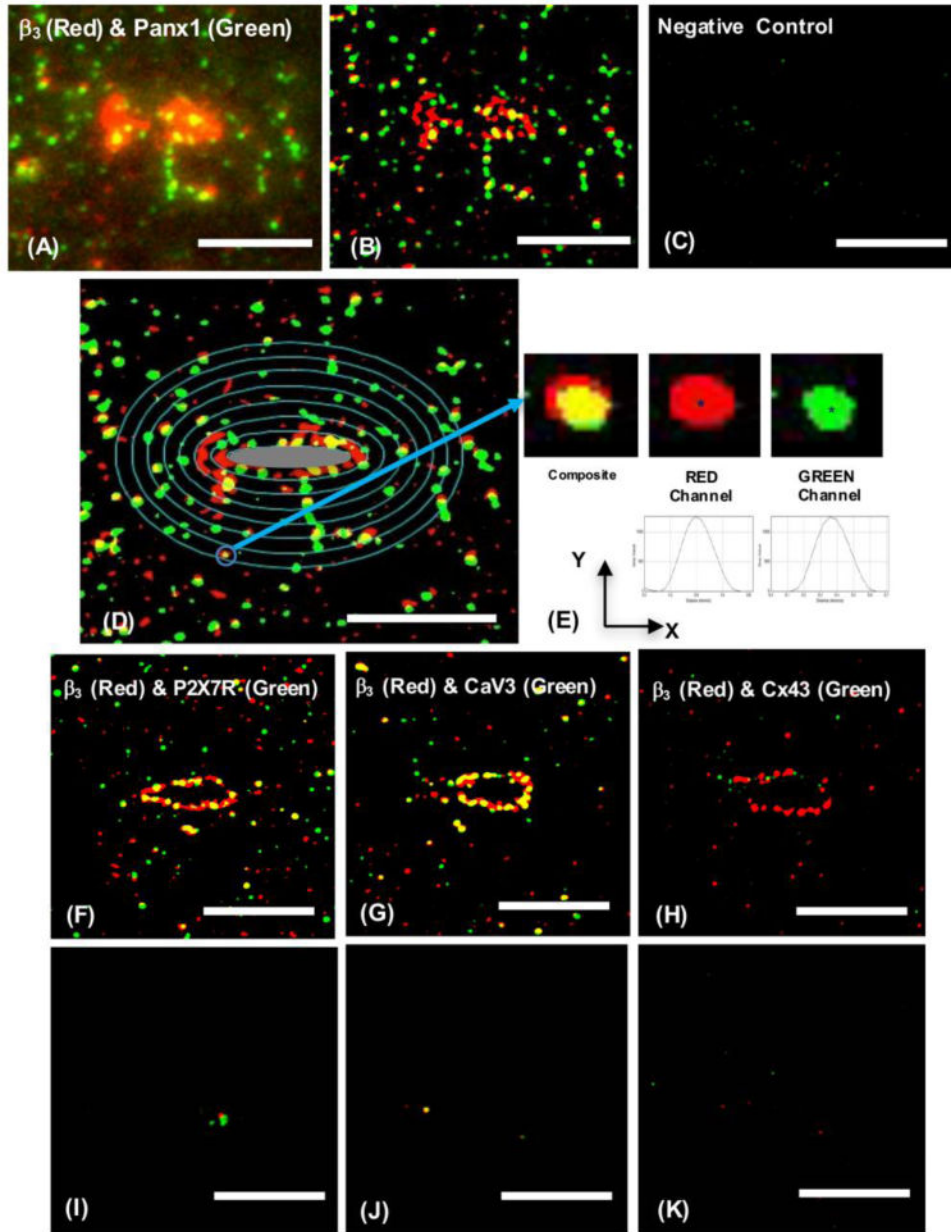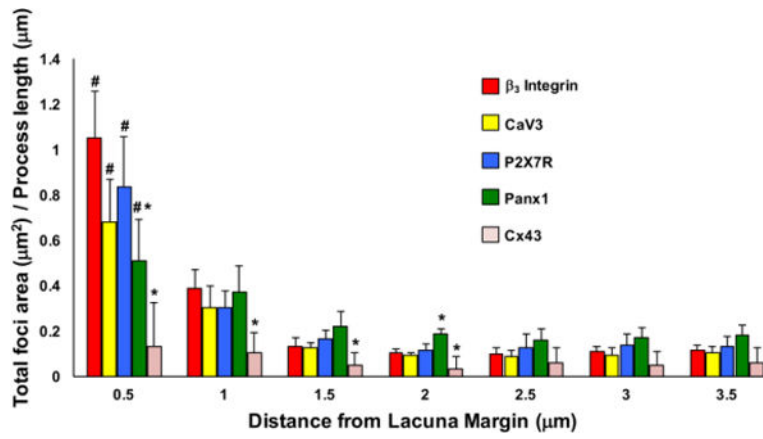
Figure 2.

(A) Wide-field fluorescence image of osteocyte double-IHC stained to detect β_3 integrin (Red, AlexaFluor568) and Panx1 (Green, AlexaFluor488), **(B)** Corresponding thresholded SIM image of the same cell shown in a single 110 nm thick optical section (see Fig 1 for explanation of discontinuous appearance of cell processes in these very thin optical sections); **(C)** Negative control with non-immune species specific IgGs. **(D)** is the same image as in **B**, shown with concentric ellipses every 0.5 μm that were used in standardized sampling of staining foci on cell processes as a function of distance from the lacunar edge; the central gray oval represents the osteocyte lacunar edge and measurements were started 0.5 μm away from the edge. Note that this image has been rotated slightly counterclockwise compared to **B**, in order to place the osteocyte long axis in the horizontal plane. **(E)** Example

of a composite stain locus, magnified (blue arrow) and shown in separate Red and Green component channels. Asterisks show the X, Y-location of the maximum intensity, which were used to determine distances. (**F-H**) show one optical plane of thresholded SIM images of β_3 integrin (Red) vs P2X7R (Green), β_3 integrin (Red) vs CaV3 (Green) and β_3 integrin (Red) vs Cx43 (Green), respectively, and (**I-K**) negative controls (non-immune species specific IgGs) corresponding to the staining pair in the image shown immediately above. Scale bar = 5 μm.
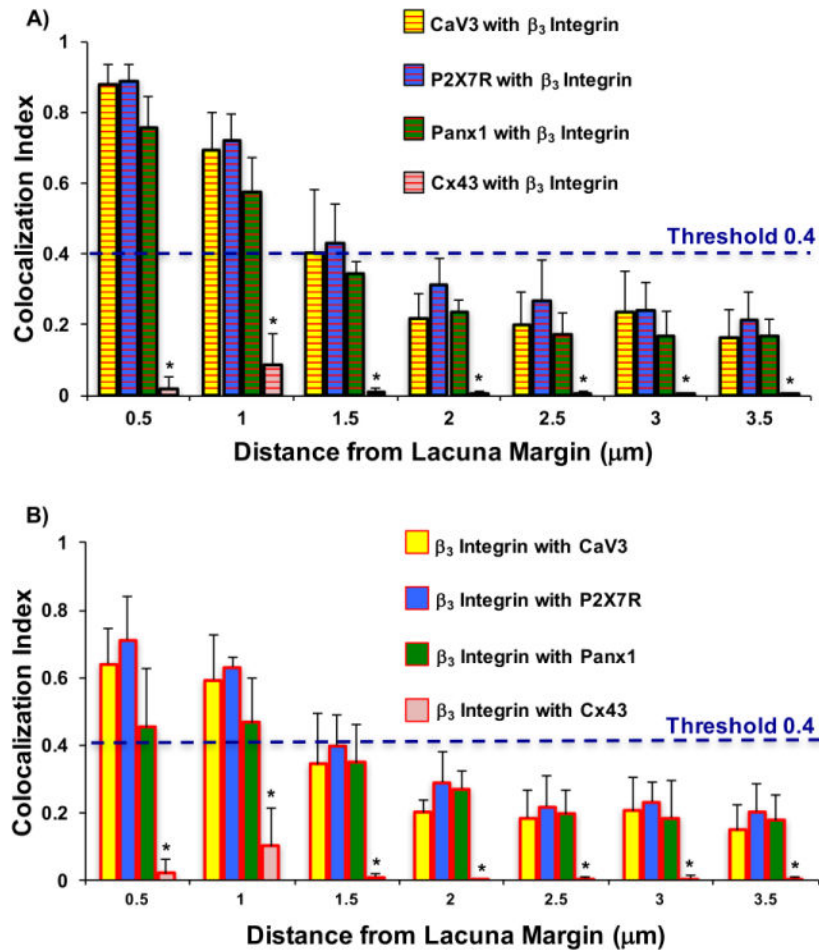
Figure 3.
SIM image of osteocytes with double–IHC staining for β_3 integrin (Red) and Vinculin (Green). Vinculin staining was found at osteocyte cell bodies (green arrows), but not in osteocyte processes. Only β_3 integrin was found on osteocyte processes (white arrows).
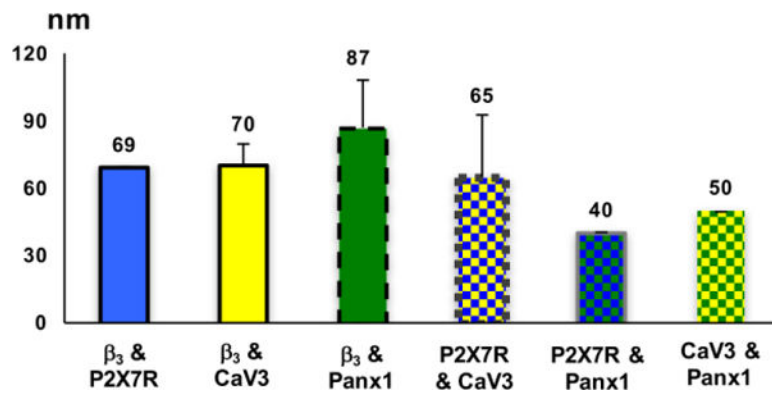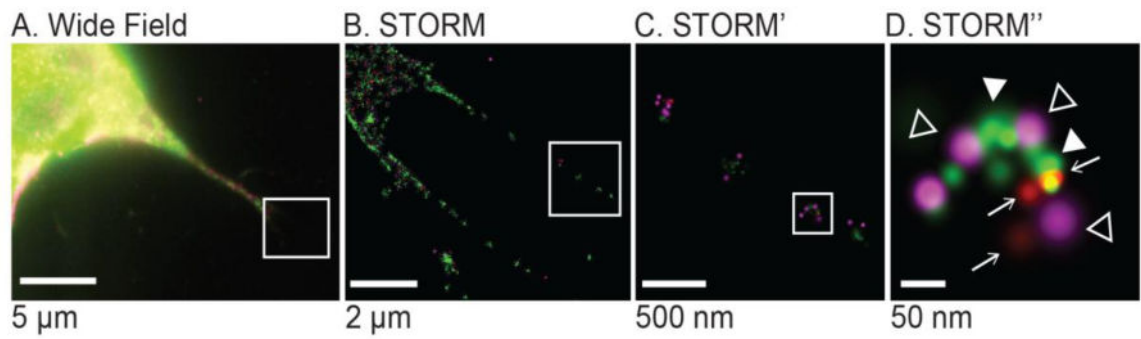
Figure 4.
Distribution of candidate proteins along osteocyte processes plotted with respect to distance from the lacuna margin. ($p<0.05$ for # versus distal locations >1.5um, * versus β_3 integrin)

Figure 5.
(**A**) Manders Coefficients for CaV3, P2X7R and Panx1 colocalizations with β_3 integrin foci along osteocyte processes, plotted with respect to distance from the lacuna ($p<0.05$ for * vs β_3 integrin with CaV3, P2X7R and Panx1 pair values) (**B**). Reverse Manders Coefficients for β_3 integrin foci colocalizations with CaV3, P2X7R and Panx1along osteocyte processes, plotted with respect to distance from the lacunar margin. $p<0.05$ for * vs β_3 integrin with CaV3, P2X7R and Panx1 pair values

Figure 6.
Distance between candidate membrane; data shown as mean ± SD as measure from SIM image maps.

Figure 7.
(**A**) Wide field image of MLOY-4 osteocyte. (**B-D**) STORM images. Green: β₃-integrin, filled arrowheads, red: P2X7, arrows, magenta: Panx1-mCherry, open arrowheads. (Panx1-mCherry is magenta, P2X7-AF647 is red, and Integrin-Flag-AF488 is green)

Table 1

Antibodies Used in Co-Localization Studies

EXPERIMENT	TARGET	1° ANTIBODY	VENDOR	2° ANTIBODY	VENDOR
Pilot	β_3 integrin	#ab20146	Abcam	# A-32723 AlexaFluor488	ThermoFisher
β_3 integrin vs Vinculin	β_3 integrin	# ab20146	Abcam	#A-11019 AlexaFluor568	ThermoFisher
β_3 integrin vs Vinculin	Vinculin	#V9131	Sigma	#A-11034 AlexaFluor488	ThermoFisher
β_3 integrin vs Panx1,P2X7R,CaV3	β_3 integrin	# ab75872	Abcam	#A-10042 AlexaFluor568	ThermoFisher
β_3 integrin vs Panx1	Panx1	#SC-49695	SantaCruz	#A-11055 AlexaFluor488	ThermoFisher
β_3 integrin vs P2X7R	P2X7R	# ab93354	Abcam	#A-11055 AlexaFluor488	ThermoFisher
β_3 integrin vs CaV3	Cav3	# SC-16263	SantaCruz	#A-11055 AlexaFluor488	ThermoFisher
β_3 integrin vs Cx43	Cx43	#C6219	Sigma	#A-11034 AlexaFluor488	ThermoFisher
Panx1 vs P2X7R,	Panx1	#SC-49693	SantaCruz	#A11055 AlexaFluor488	ThermoFisher
Panx1 vs CaV3	Panx1	#ab139715	Abcam	#A-10042 AlexaFluor568	ThermoFisher
Panx1 vs P2X7R P2X7R vs CaV3	P2X7R	#ab109246	Abcam	#A-10042 AlexaFluor568	ThermoFisher
Panx1 vs CaV3	Cav3	#SC-16263	SantaCruz	#A-11055 AlexaFluor488	ThermoFisher
STORM	FLAG	F3165, mouse	Sigma	AlexaFluor488	